BIOCHEMISTRY
including biophysical chemistry & molecular biology

ARTICLE

pubs.acs.org/biochemistry

Modification of Akt2 by 4-Hydroxynonenal Inhibits Insulin-Dependent Akt Signaling in HepG2 Cells

C. T. Shearn, K. S. Fritz, P. Reigan, and Dennis R. Petersen*

Department of Pharmaceutical Sciences, University of Colorado—Denver, Aurora, Colorado 80045, United States

Supporting Information

ABSTRACT: The production of reactive aldehydes such as 4-hydroxy-2-nonenal (4-HNE) is a key component of the pathogenesis in a spectrum of hepatic diseases involving oxidative stress such as alcoholic liver disease (ALD). One consequence of ALD is increased insulin resistance in hepatocytes. To understand the effects of 4-HNE on insulin signaling in liver cells, we employed a model using hepatocellular carcinoma cell line HepG2. Previously, we have demonstrated an increase in the level of Akt phosphorylation is mediated by 4-HNE inhibition of PTEN, a direct regulator of Akt. In this work, we evaluated the effects of 4-HNE on insulin-dependent stimulation of the Akt2 pathway. We demonstrate that 4-HNE selectively leads to phosphorylation of Akt2. Although Akt2 is phosphorylated following 4-HNE treatment, the level of downstream phosphorylation of Akt substrates such as GSK3β and MDM2 is significantly decreased. Pretreatment with 4-HNE prevented insulin-dependent Akt signaling and decreased intracellular Akt activity by 87%. Using biotin hydrazide capture, it was confirmed that 4-HNE treatment of cells resulted in carbonylation of Akt2, which was not observed in untreated control cells. Using a synthetic GSK3α/β peptide as a substrate, treatment of recombinant human myristoylated Akt2 (rAkt2) with 20 or 40 μM 4-HNE inhibited rAkt2 activity by 30 or 85%, respectively. Matrix-assisted laser desorption ionization time-of-flight tandem mass spectrometry (MALDI-TOF/TOF) identified Michael addition adducts of 4-HNE with His196, His267, and Cys311 of rAkt2. Computation-based molecular modeling analysis of 4-HNE adducted to His196 and Cys311 of Akt2 suggests inhibition of GSK3β peptide binding by 4-HNE in the Akt2 substrate binding pocket. The inhibition of Akt by 4-HNE provides a novel mechanism for increased insulin resistance in ALD. These data provide a potential mechanism of dysregulation of Akt2 during events associated with sustained hepatocellular oxidative stress.

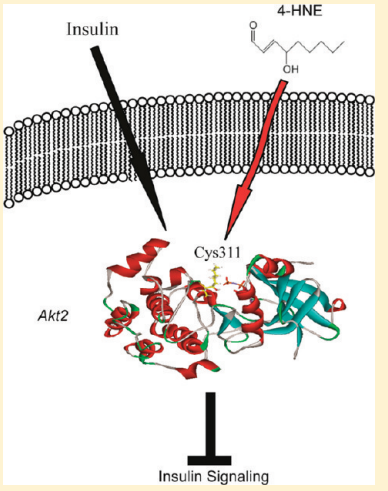

Oxidative modification of proteins by reactive aldehydes in the liver has been implicated in an increasing number of disease states, including primary biliary cirrhosis, hepatitis C, and chronic alcoholic liver disease (ALD).[1−4] A primary marker for measuring increased oxidative stress in cells is the presence of 4-hydroxy-2-nonenal (4-HNE), the level of which is increased in chronic metabolic liver diseases such as non-alcoholic steatohepatitis (NASH) and ALD.[5,6] Reactive aldehydes such as 4-HNE arise from peroxidation of lipids, including linoleic acid within membranes.[7] Although overall concentrations of 4-HNE are probably in the micromolar or submicromolar range, it has been calculated that concentrations within lipid bilayers could approach 3.8−100 mM.[8,9] 4-HNE is an electrophile that will react with protein nucleophiles, including Cys, Lys, and His residues of proteins such as phosphatase and tensin homologue from which chromosome 10 has been deleted (PTEN), tubulin, and peroxiredoxin 6.[10−12]

The Akt kinase pathway plays a critical role in the regulation of cell growth, survival, and proliferation. There are three different mammalian isoforms of Akt [Akt1, Akt2, and Akt3 (PKBα, -β, and -γ, respectively)]. Although these isoforms are encoded on different genes, they are more than 80% identical in amino acid sequence. All three isoforms require phosphatidylinositol 3-kinase (PI3K)-dependent production of phosphatidylinositol 3,4,5-trisphosphate [PtdIns(3,4,5)P_3] for activation. In addition, the three isoforms also contain an N-terminal pleckstrin homology (PH) domain (approximately amino acids 1−133), a kinase domain (approximately amino acids 150−448), and a hydrophobic motif (approximately amino acids 449−481). As with other AGC kinases, within the kinase domain, there is an activation loop (amino acids 298−310) that regulates access of the substrate and ATP. All three of these domains are necessary for full activation of Akt within the cell. Activation requires recruitment of Akt2 to the membrane via its PH domain; normally, the PH domain is in a PH-in orientation because of an association of the PH domain with the Akt active site.[13] This conformation blocks access of PDK1 to Thr309.[14] Membrane binding leads to a conformational change in the PH domain leading to a PH-out conformation with movement of the activation loop and exposure of Thr309 to PDK1. In the inactive

Received: January 6, 2011
Revised: February 28, 2011
Published: March 25, 2011

state, the ATP binding site is sterically hindered by the presence of the activation loop. Phosphorylation of Thr309 in combination with phosphorylation of Ser474 further exposes the active site allowing for catalysis.[15] Following activation, Akt phosphorylates a variety of proteins required for growth and survival, including glycogen synthase kinase 3β (GSK3β) and the ubiquitin ligase murine double minute oncogene 2 (MDM2). Akt can be inactivated via two different mechanisms, PTEN-catalyzed dephosphorylation of PtdIns(3,4,5)P_3 to PtdIns(4,5)P_2 and protein phosphatase-mediated dephosphorylation of Thr308 and Ser473 by protein phosphatase 2A (PP2A) and PH domain and leucine rich repeat protein phosphatases (PHLPP), respectively.[16]

Within the liver, insulin is a key mediator in lipid accumulation and glucose homeostasis.[17,18] Insulin binds to the insulin receptor, initiating a cascade involving insulin receptor substrate 1 and 2 (IRS-1 and IRS-2, respectively), production of PtdIns(3,4,5)P_3 via PI3K, and subsequent activation of Akt2.[18] The treatment of adipocytes with siRNA specific for Akt2 has been shown to modulate glucose transporter type 4 (Glut4) translocation and glucose uptake.[19] Although Akt2 specific targets are difficult to delineate, activation of Akt2 leads to phosphorylation and/or inactivation of GSK3β and an increased level of glycogen synthesis.[19] In cell culture models, Akt2 phosphorylation of MDM2 regulates p53 stability and resistance to anoikis.[20]

In the liver, deletion of Akt2 inhibits insulin-dependent signaling associated with dysregulation of glucose homeostasis associated with insulin resistance.[21] Hepatocyte specific deletion of phosphatase and tensin homologue (PTEN) constitutively activates Akt and produces a dramatic increase in the level of lipid accumulation and steatosis.[22] These phenotypes were not present when the PTEN knockout mice were subsequently crossed with Akt2 hepatocyte specific knockout mice, further implicating Akt2 in the regulation of insulin signaling in mice.[23] In other studies, acute ethanol exposure inhibits insulin signaling in the liver via a reduced level of formation of p-Akt and impaired Akt-dependent survival signaling.[24] Although mechanisms of total Akt inactivation via dephosphorylation have been explored, the effects of 4-HNE on Akt signaling have not been examined in hepatocyte models.[25]

Previously, we have demonstrated that in hepatocytes, the lipid phosphatase PTEN is carbonylated by 4-HNE, leading to inhibition of PTEN activity and subsequent Akt phosphorylation.[12] In the work presented here, we describe the effects of 4-HNE on Akt2 signaling and its ability to phosphorylate GSK3β and MDM2 in the context of insulin stimulation. Specifically, we find that 4-HNE inhibits insulin stimulation of the Akt2 pathway and direct modification of recombinant Akt2 by 4-HNE inhibits its activity.

EXPERIMENTAL PROCEDURES

Treatment of HepG2 Cells. HepG2 cells were maintained at 50−80% confluence in RPMI supplemented with 10% fetal bovine serum, 100 mM Hepes, 100 IU/mL penicillin, and 100 g/mL streptomycin. Cells were plated into six-well plates at a density of 1×10^6 cells/well. The following day, the cells were washed twice in serum free RPMI and treated with the indicated doses of 4-HNE. For insulin treatments, cells were treated with 100 mM 4-HNE for 60 min and washed once in serum free medium, and insulin (Sigma-Aldrich, St. Louis, MO) (100 nM for 15 min) was added.

Western Blotting. Cells were lysed for 5 min in 50 mM HEPES, 100 mM NaCl, 1% Triton X-100, 2 mM EDTA (pH 7.7), and protease inhibitors (Sigma, St. Louis, MO), followed by sonication for 3×10 s. For each gel, 10 μg of whole cell lysates was loaded per well on 7% SDS−PAGE gels, electroblotted to PVDF, blocked in Tris-buffered saline with 1% Tween (TBST) and 5% nonfat dry milk for 1 h, and incubated overnight with a primary antibody. The following primary antibodies were used at 1:1000 dilutions in TBST: rabbit polyclonal, p-Akt (Ser473), total Akt, p-MDM2 (Ser166), p-GSK3β (Ser9), GSK3β (Cell Signaling, Danvers, MA, catalog nos. 4060, 4691, 3521, 9323, and 9315); mouse monoclonal, actin (1:5000, Sigma, catalog no. A5441), Akt2 (1:1000, Cell Signaling, catalog no. 5329), Akt1 (1:1000, Cell Signaling, catalog no. 2967), total MDM2 (ABCAM AB-10567), p-glycogen synthase (Ser641) (Millipore, Temecula, CA, catalog no. 07-817), total glycogen synthase (1:1000, Millipore, catalog no. 04-357). The rabbit polyclonal 4-HNE antibody was used at a 1:1000 dilution as previously described.[11] The following morning blots were washed three times for 5 min in TBST and incubated for 1 h in horseradish peroxidase-conjugated goat polyclonal anti-rabbit secondary antibody or donkey polyclonal anti-mouse secondary antibody (1:5000) (Jackson ImmunoResearch Laboratories, West Grove, PA). Blots were washed three times for 5 min in TBST and subsequently developed using chemiluminescence (Pierce Supersignal, Thermofisher Scientific, Rockford, IL). All Western blots were quantified using NIH Image J.

Akt Activity Assays. The Akt activity assay was purchased and utilized the immunoprecipitation of p-Akt (Ser473) according to the manufacturer's instructions (Cell Signaling, catalog no. 9480). Briefly, cells were treated with 100 μM 4-HNE for 60 min, 100 nM insulin for 15 min, or both and lysed, and p-Ser473 Akt immunoprecipitated from 150 μg of total lysates. Akt activity was determined by in vitro phosphorylation of a GST-GSK3α/β fusion protein (1 μg/assay) in the presence of 1 mM ATP, followed by detection via Western blotting using anti-phospho GSK3α/β polyclonal antibodies. For rAkt2 activity, 0.5 μg of purified rAkt2 was substituted in the assay via replacement of the immunoprecipitated p-Ser473 Akt.

Biotin Hydrazide Modification of Alkylated Akt2. To evaluate reactive aldehyde adduction, 1×10^7 HepG2 cells were treated with 100 μM 4-HNE for 1 h. Cells were then lysed in 50 mM HEPES, 100 mM NaCl, 2 mM EDTA, and 2.5 mM biotin hydrazide. To remove excess biotin, lysates were dialyzed overnight at 4 °C. Biotinylated proteins were pulled down via incubation with streptavidin agarose beads (Pierce) on a rotary mixer at 4 °C for 3 h, washed five times in PBS, loaded onto SDS−PAGE gels, and processed according to Western blotting protocols.

Adduction and Trypsin Digest of Recombinant myrAkt2 by 4-HNE. Five micrograms of rAkt2 was treated with 4-HNE at molar ratios of 0.1, 1:1, 2.5:1, 5:1, 10:1, and 20:1 for 30 min at 37 °C; 0.5 μg was removed, loaded onto an SDS−PAGE gel, and Western blotted using anti-4-HNE polyclonal antibodies. To verify Akt2 adduction, membranes were then stripped for 15 min using Restore stripping buffer (Pierce, Rockford, IL), washed twice in TBST, and blocked once again for 1 h in TBST 5% NFDM. After being blocked, membranes were incubated overnight with mouse anti-Akt2 (Cell Signaling, catalog no. 5329) and subsequently processed. The rest of the sample was

treated with 10 mM sodium borohydride in 100 mM NaOH for 30 min at 37 °C. Samples were boiled in 5× SDS loading buffer and subjected to SDS−PAGE. Gels were stained for 15 min with Coomassie Blue R250 and destained overnight in 10% acetic acid and 20% MEOH run on a 7.5% SDS−PAGE gel and Coomassie stained or destained overnight. From the gel, each band was picked and destained in 50 mM NH_4HCO_3 for an additional
24 h. Gel slices were dehydrated with 100% ACN for 15 min, reduced in 10 mM DTT and 50 mM NH_4HCO_3 for 45 min at 60 °C, and alkylated in 50 mM iodoacetic acid in 50 mM NH_4HCO_3 for 45 min in the dark at room temperature. Samples were washed once in 50 mM NH_4HCO_3 and digested in 0.3 μg of trypsin with 50 mM NH_4HCO_3 overnight. Peptide extraction consisted of sonicating for 20 min in 50% acetonitrile and 50 mM NH_4HCO_3 followed by sonication in 5% formic acid in acetonitrile for an additional 20 min. Samples were dried down and resuspended in 0.1% trifluoroacetic acid.

MALDI-TOF/TOF Characterization of 4-HNE-Modified Akt2. Recombinant Akt2 was incubated with increasing ratios of 4-HNE. Samples were run on a 10% SDS−PAGE gel, excised, and digested with trypsin according to published methods. The samples were prepared using C18 ZipTips (Millipore, Billerica, MA), mixed 1:1 with α-cyano-4-hydroxycinnamic acid (CHCA, 10 mg/mL), and spotted in 1 μL aliquots onto an Opti-TOF 384 well insert (Applied Biosystems, Foster City, CA). An ABI 4800 Plus MALDI-TOF/TOF instrument (Applied Biosystems) was used to characterize the adduction of rAkt2 by 4-HNE. The mass spectrometer was operated for peptide analysis using a laser power of 2500 with calibration using a ProteoMass Calibration Kit (Sigma). Collision-induced dissociation (CID) MS/MS was performed at 1 kV, and the collision gas was air. MS/MS spectra were recorded using a laser power of 3500 with 2000 laser shots or until a minimal signal-to-noise ratio was reached. Data analysis was performed using Mascot version 2.1.04 (http://www.matrixscience.com) and Applied Biosystems 4000 Series Explorer version 3.5, and b/y peptide ion fragmentation was predicted and compared with experimental MS/MS data using ProteinProspector version 5.4 (http://prospector.ucsf.edu, UCSF Mass Spectrometry Facility).

Molecular Modeling. All simulations were performed using Discovery Studio version 2.5.5 (Accelrys Inc., San Diego, CA). The crystallographic coordinates of the 1.6 Å human activated Akt crystal structure (Protein Data Bank entry 1O6L) were obtained from the Protein Data Bank (http://wwww.rcsb.org).[26] The 4-HNE modification of the Cys311 residue of Akt was typed with the CHARMm force field and subjected to minimization (1000 iterations) using the conjugate gradient method to a convergence of 0.001 kcal/mol using the generalized Born implicit solvent model.[27,28]

RESULTS

The Extent of 4-HNE Modification of HepG2 Proteins Increases via a Time-Dependent Mechanism. To characterize the overall propensity of 4-HNE to modify proteins within the cell, we used a 2 h time course. It is apparent from the Western blot presented in Figure 1A that 100 μM 4-HNE leads to a time-dependent increase in a spectrum of 4-HNE reactive proteins. A comparison between the Western blot and a Coomassie-stained gel (Figure 1B) indicates selective modification of proteins following 4-HNE treatment. Densitometric analysis of total

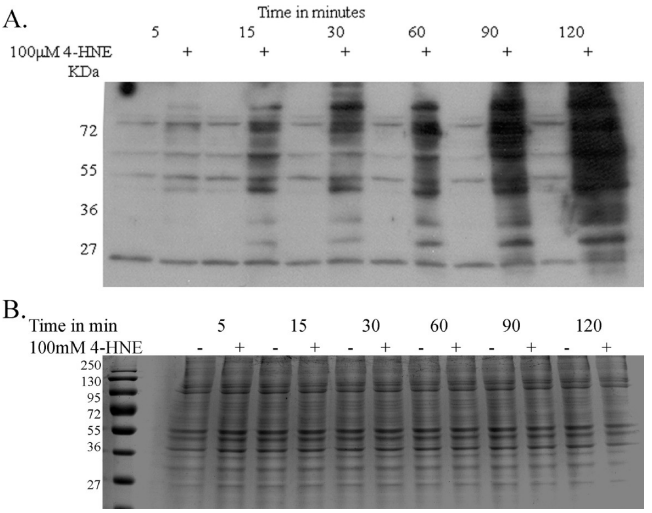

Figure 1. Effects of 4-HNE on proteins in HepG2 cells. (A) Representative immunoblot demonstrating the time-dependent increase in the level of 4-HNE reactive proteins. HepG2 cells were treated with 100 μM 4-HNE (5−120 min), lysed, and examined via Western blotting using rabbit polyclonal anti-4-HNE antibodies. (B) Coomassie-stained gel of the time course of 4-HNE-treated HepG2 cells.

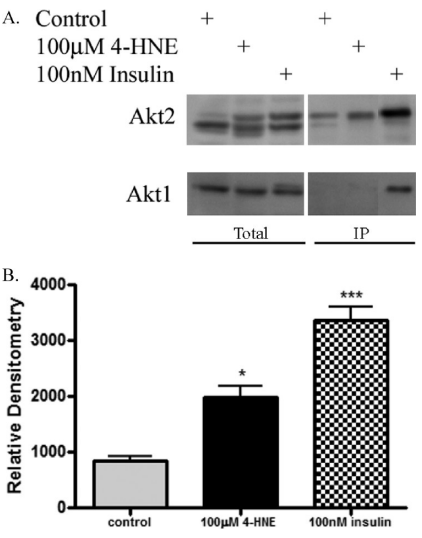

Figure 2. 4-HNE specific activation of Akt2 in HepG2 cells. (A) HepG2 cells were treated with 100 nM insulin (15 min) or 100 μM 4-HNE (60 min). Cells were lysed, and 150 μg of total lysate immunoprecipitated using p-Ser473 Akt polyclonal antibodies. Immunoprecipitates (IP) were subjected to 8% SDS−PAGE, blotted, and probed for Akt1 and Akt2. (B) Quantification of 4-HNE-mediated p-Ser473 Akt. This experiment was performed in at least triplicate and subjected to one-way analysis of variance with Tukey's multiple-comparison test (*$p < 0.05$; ***$p < 0.001$).

4-HNE reactive bands at the 2 h time point indicates a 7-fold increase in the level of 4-HNE-modified proteins compared to control (data not shown).

Akt2 Is Preferentially Phosphorylated following 4-HNE Treatment in HepG2 Cells. Previous studies indicated that Akt is phosphorylated following 4-HNE treatment in both HepG2 cells and primary hepatocytes.[12] To identify the specific Akt isoform phosphorylated, total p-Akt (Ser473,4) was immunoprecipitated

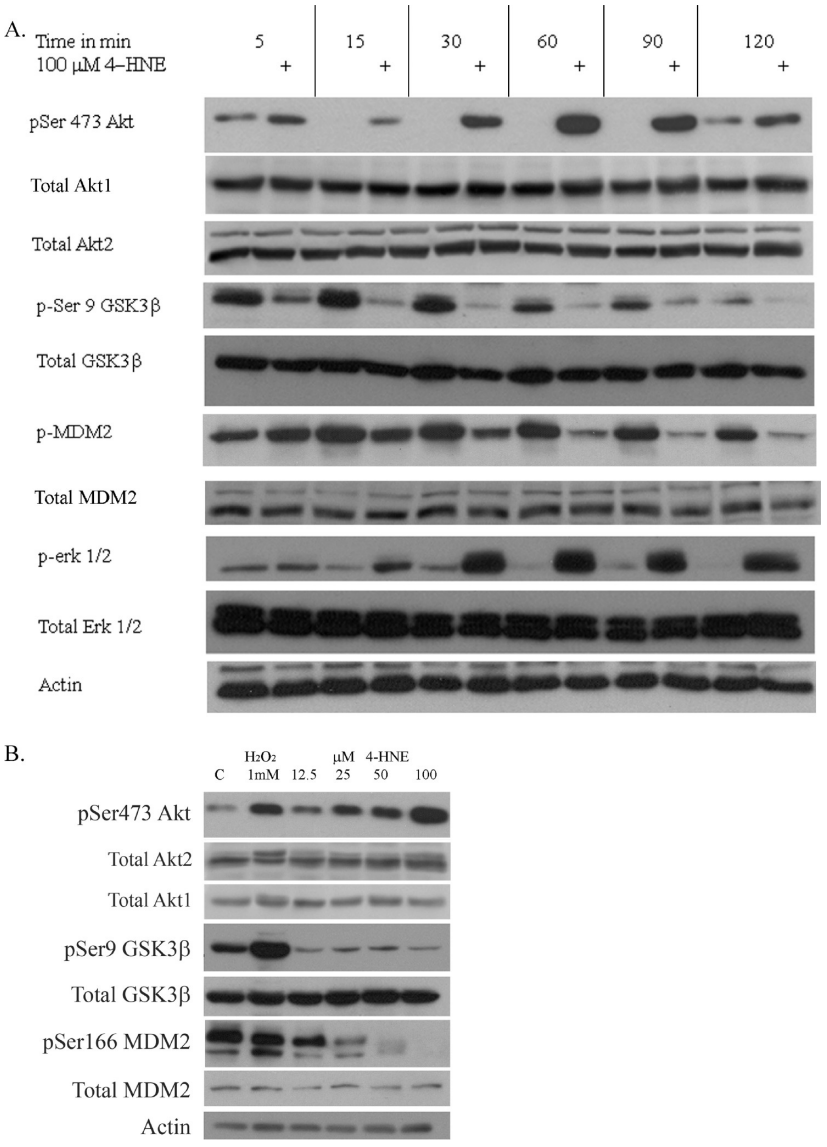

Figure 3. Effects of 4-HNE on Akt-dependent downstream signaling. (A) Time-dependent activation of Akt. HepG2 cells were treated for 5−120 min. Cells were lysed and examined via 7% SDS−PAGE and Western blotting using p-Akt (Ser473), Akt2, p-GSK3β (Ser9), GSK3β, p-MDM2 (Ser166), MDM2, p-Erk1/2, Erk1/2, and actin (note that film exposures for p-Ser473 Akt are 1 min). (B) Concentration-dependent inhibition of Akt signaling. HepG2 cells were treated with increasing concentrations of 4-HNE (0−100 μM for 60 min) or 1 mM hydrogen peroxide (5 min). Cells were lysed and examined as described above. Blots are representative of at least three independent experiments.

from HepG2 cells treated with either insulin or 100 μM 4-HNE and analyzed by Western blot using Akt isoform specific antibodies. Data presented in Figure 2A show that insulin stimulates phosphorylation of both Akt1 and Akt2. Interestingly, 4-HNE stimulates phosphorylation of only Akt2 [Akt3 could not be detected in HepG2 lysates (data not shown)]. The densitometric analysis presented in Figure 2B reflects a statistically significant 2-fold increase in the level of Akt2 phosphorylation compared to controls (Figure 2B). Collectively, these results demonstrate 4-HNE-dependent phosphorylation of Akt2.

The Level of Phosphorylation of Downstream Substrates of Akt2 Is Significantly Reduced following 4-HNE Exposure. To evaluate the effects of 4-HNE on Akt2-dependent signaling, HepG2 cells were treated with 100 μM 4-HNE for 5−120 min. Lysates were examined for an increased level of phosphorylation of downstream targets of Akt. In Figure 3A, total levels of Akt1 and Akt2 do not change in response to 4-HNE. Surprisingly, although Akt2 is clearly phosphorylated, the level of phosphorylation of its direct downstream substrate, GSK3β, is decreased. To verify the absence of Akt-dependent downstream phosphorylation, the phosphorylation status of MDM2 was subsequently examined. As seen with GSK3β, a time-dependent decrease in the level of phosphorylation of p-MDM2 (Ser166) was evident compared to controls. These results indicate that although Akt2 is phosphorylated, phosphorylation of downstream targets of Akt2 is suppressed following 4-HNE treatment.

Previous research has demonstrated phosphorylation of Akt following 4-HNE treatment via both concentration- and time-dependent mechanisms.[12] To determine the effects of 4-HNE on Akt-dependent downstream signaling, HepG2 cells were incubated with increasing concentrations of 4-HNE (0−100 μM) for 1 h and the phosphorylation status of downstream targets of Akt

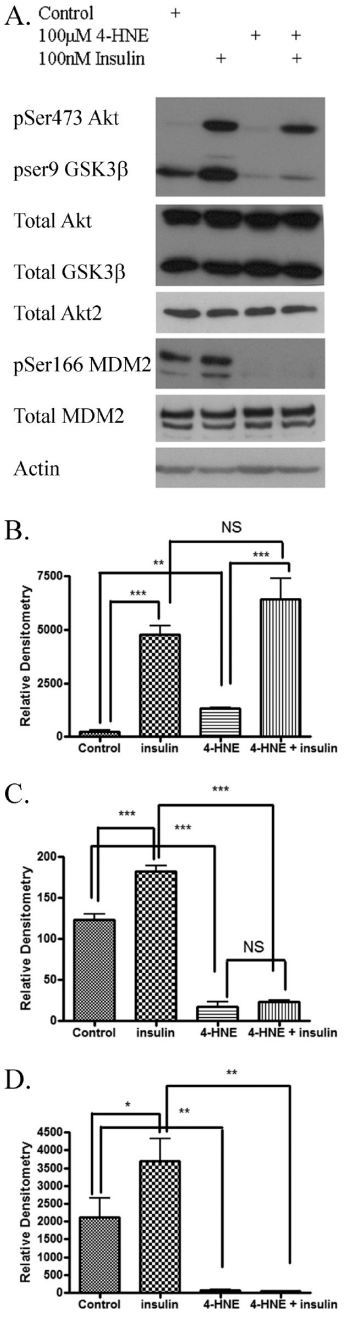

Figure 4. Inhibition of insulin-dependent Akt signaling by 4-HNE. Cells were treated in serum free medium with 100 μM 4-HNE or control for 60 min, washed in serum free medium, and stimulated with 100 nM insulin for 15 min. Cells were lysed and processed as described in Experimental Procedures. (A) Western blot using antibodies for the following proteins: Akt (Ser473), Akt2, p-GSK3β (Ser9), GSK3β, p-MDM2 (Ser166), MDM2, p-GSK3α/β (Akt activity assay), and actin (note that film exposures for p-Ser473 Akt are less than 2 s). (B–D) Quantification of blots depicted in panel A: p-Akt (Ser473) (B), p-GSK3β (Ser9) (C), and p-MDM2 (Ser166) (D). Each blot is representative of three independent experiments, for MDM2 samples were subjected to 5% SDS–PAGE and all other samples were subjected to 7% SDS–PAGE. Statistical analysis occurred via one-way analysis of variance with Tukey's multiple-comparison test ($^*p < 0.05$; $^{**}p < 0.01$; $^{***}p < 0.001$).

such as GSK3β and MDM2 were examined. The data in Figure 3B demonstrate following 4-HNE treatment, however,

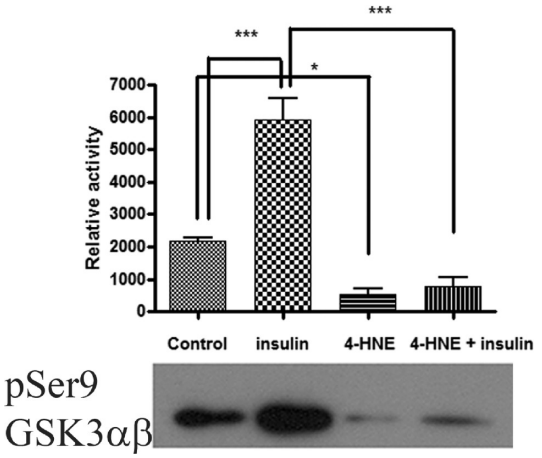

Figure 5. Inhibition of Akt activity by 4-HNE in HepG2 cells. Western blot and quantification of the in vitro Akt activity assay using a synthetic GSK3$\alpha\beta$ peptide and samples described in the legend of Figure 4. All samples were assessed in triplicate. Statistical analysis occurred via one-way analysis of variance with Tukey's multiple-comparison test ($^*p < 0.05$; $^{***}p < 0.001$).

phosphorylation of GSK3β (Ser9) is clearly suppressed at all concentrations of 4-HNE and phosphorylation of MDM2 (Ser166) is inhibited in a concentration-dependent manner. Total levels of both Akt1 and Akt2 did not change significantly. As expected, the positive control (1 mM hydrogen peroxide) stimulated a marked increase in the level of phosphorylation of both GSK3β (Ser9) and MDM2 (Ser166). These data indicate concentration-dependent suppression of Akt signaling by 4-HNE in HepG2 cells.

Erk1/2 is not a direct target of Akt2 but is involved in cellular growth and proliferation.[29] To examine phosphorylation of a non-Akt-dependent substrate, the ability of 4-HNE to modulate Erk1/2 phosphorylation was examined (Figure 3A). Following 4-HNE treatment, a time-dependent increase in the level of Erk1/2 phosphorylation was observed. These observations suggest that 4-HNE activates multiple pathways and the ability of 4-HNE to inhibit Akt2 downstream signaling is pathway specific.

4-HNE Inhibits Insulin Signaling in HepG2 Cells. Akt2 plays an important role in hepatocyte insulin signaling.[17] To assess the direct effects of 4-HNE on insulin signaling, we pretreated HepG2 cells with 4-HNE followed by stimulation with insulin (Figure 4A–D). The results presented in Figure 4A show that total levels of Akt and Akt2 are unchanged following both insulin and 4-HNE treatment. Akt2 is also phosphorylated at Ser474 following insulin stimulation. Analysis of Akt downstream targets p-GSK3β (Ser9) and p-MDM2 (Ser166) clearly indicates increased levels of phosphorylation following insulin stimulation. Using 4-HNE alone, the level of phosphorylation of Akt significantly increased by 3-fold over controls (Figure 4A). The level of phosphorylation of both GSK3β and MDM2 significantly decreased following 4-HNE compared with both the control and the insulin-stimulated cells.

It is apparent from Figure 4A that 4-HNE treatment clearly blocks Akt downstream signaling in HepG2 cells; to improve our understanding of the inhibitory effects of 4-HNE, we preincubated cells with 4-HNE followed by insulin stimulation. In the 4-HNE/insulin combined cells, 4-HNE did not have a significant effect on Ser473 Akt phosphorylation (Figure 4B). However, the

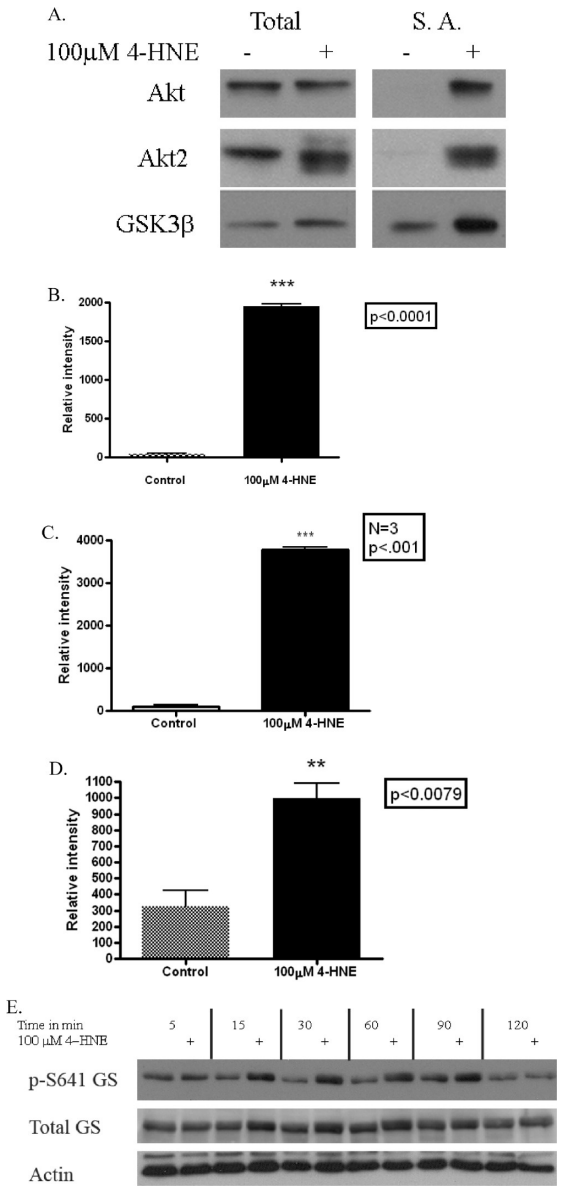

Figure 6. Akt2 is modified by reactive aldehydes following 4-HNE treatment in HepG2 cells. (A) Streptavidin (S.A.) pull-down of 4-HNE-modified Akt and Akt2 from HepG2 cells. Protein (125 μg) from 4-HNE-treated (100 μM/60 min in serum free medium) or untreated cells was incubated for 2 h with 2.5 mM biotin hydrazide, dialyzed, and purified using streptavidin pull-down. Samples were subsequently analyzed using SDS−PAGE and Western blotting with a rabbit polyclonal anti-Akt2, pan-Akt, or anti-GSK3β antibody. (B−D) Densitometric analysis and quantification of Western blots: pan-Akt (B), Akt2 (C), and GSK3β (D). All samples were assessed in triplicate. Statistical analysis occurred via one-way analysis of variance (***p < 0.001). (E) Time-dependent phosphorylation of Ser641 on glycogen synthase in 4-HNE-treated HepG2 cells.

level of phosphorylation of the Akt downstream target GSK3β (Ser9) was significantly decreased by 86 and 87% compared with those of control and insulin-stimulated cells, respectively (Figure 4C). Examination of the phosphorylation of the Akt substrate MDM2 indicated a dramatic decrease in p-MDM2 (Ser166) by 97 and 98% compared with those of control and insulin-treated cells, respectively (Figure 4D). Taken together,

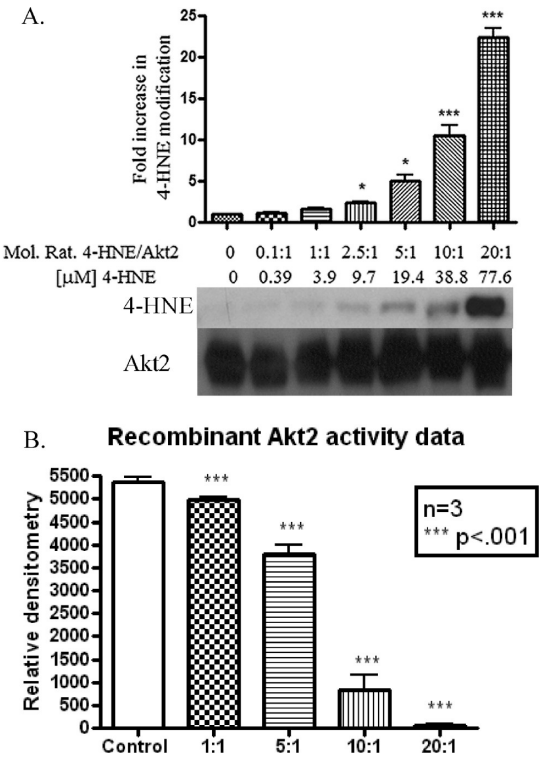

Figure 7. Effects of 4-HNE on recombinant myrAkt2. (A) Western blotting of rAkt2 treated with 4-HNE. Purified rAkt2 was incubated with increasing molar ratios of 4-HNE for 30 min at room temperature. Samples were boiled in 5× SDS loading buffer, subjected to 8% SDS−PAGE, blotted, and probed for 4-HNE using anti-4-HNE polyclonal antibodies followed by stripping and reprobing for Akt2. (B) Inhibition of rAkt2 by 4-HNE. Purified rAkt2 was incubated with increasing ratios of 4-HNE, and phosphorylation assays were performed using a GST fusion GSK3α/β synthetic substrate as described in Experimental Procedures. All samples were performed in at least triplicate. Statistical analysis occurred via one-way analysis of variance with Tukey's multiple-comparison test (*p < 0.05; **p < 0.01; ***p < 0.001).

the data in Figure 4A−D show that 4-HNE mediates inhibition of insulin stimulation through GSK3β and MDM2 phosphorylation in HepG2 cells.

To examine the effects of 4-HNE on cellular Akt activity, an Akt activity assay was performed using the aforementioned samples and a synthetic Akt substrate (GST-GSK3α/β peptide). From the Western blot in Figure 5, Akt activity is clearly reduced following 4-HNE pretreatment. Quantification of the activity assay demonstrates 4-HNE-dependent inhibition of total Akt activity by 76 and 87% compared with those of the control and insulin-treated cells, respectively. Combined, these data demonstrate 4-HNE-mediated inhibition of insulin stimulation Akt2 activity in HepG2 cells.

4-HNE Treatment Leads to an Increased Level of Carbonylation of Akt2 and GSK3β in HepG2 Cells. One method of determining 4-HNE modification or carbonylation of cellular proteins is to use biotin hydrazide modification followed by streptavidin purification of the biotinylated proteins.[30] To determine if carbonylation of cellular Akt2 occurs following 4-HNE, biotin hydrazide modification of protein-bound reactive aldehydes was employed (Figure 6A). Western blot analysis of streptavidin pull-downs from biotin hydrazide-treated lysates

Table 1. Peptides Identified from Tryptic Digests of 4-HNE-Treated rAkt2[a]

start−end	observed[b]	M_r(expt)[c]	M_r(calc)[d]	sequence[e]
1−15	1825.92	1824.91	1824.97	MNEVSVIKEGWLHKR
21−25	715.38	714.38	714.39	TWRPR
26−30	683.39	682.39	682.41	YFLLK
31−39	973.44	972.44	972.46	SDGSFIGYK
40−64	2884.31	2883.31	2883.39	ERPEAPDQTLPPLNNFSVAEC(Carb)QLMK
40−64	2900.31	2899.30	2899.38	ERPEAPDQTLPPLNNFSVAEC(Carb)QLM(Ox)K
65−76	1485.78	1484.78	1484.82	TERPRPNTFVIR
77−86	1305.62	1304.61	1304.65	C(Carb)LQWTTVIER
87−96	1202.52	1201.51	1201.54	TFHVDSPDER
87−101	1933.78	1932.77	1932.84	TFHVDSPDEREEWMR
87−101	1949.78	1948.77	1948.84	TFHVDSPDEREEWM(Ox)R
97−111	1837.85	1836.84	1836.89	EEWM(Ox)RAIQM(Ox)VANSLK
102−113	1374.67	1373.66	1373.74	AIQM(Ox)VANSLKQR
114−123	1122.45	1121.44	1121.47	APGEDPMDYK
124−146	2443.03	2442.03	2442.10	C(Carb)GSPSDSSTTEEM(Ox)EVAVSKARAK
145−160	1871.87	1870.96	1870.99	AKVTMNDFDYLKLLGK
147−156	1245.54	1244.54	1244.57	VTMNDFDYLK
147−156	1261.56	1260.55	1260.57	VTM(Ox)NDFDYLK
186−202	1896.95	1895.94	1896.00	EVIIAKDEVAHTVTESR
192−202	1243.57	1242.56	1242.58	DEVAHTVTESR
192−202	1401.66	1400.65	1400.71	DEVAH(**HNE**)TVTESR
192−208	1955.03	1954.02	1953.99	DEVAHTVTESRVLQNTR
203−208	730.4	729.40	729.41	VLQNTR
209−216	926.52	925.51	925.54	HPFLTALK
217−224	1037.46	1036.45	1036.47	YAFQTHDR
225−243	2248.89	2247.89	2248.04	LCFVM(Ox)EYANGGELFFHLSR
225−243	2290.00	2288.99	2289.07	LC(Carb)FVMEYANGGELFFHLSR
225−243	2305.98	2304.97	2305.07	LC(Carb)FVM(Ox)EYANGGELFFHLSR
244−253	1292.62	1291.61	1291.66	ERVFTEERAR
246−251	780.37	779.36	779.38	VFTEER
254−269	1854.87	1853.87	1853.93	FYGAEIVSALEYLHSR
254−269	2013.00	2012.00	2012.06	FYGAEIVSALEYLH(**HNE**)SR
270−274	651.32	650.32	650.34	DVVYR
275−285	2388.98	2387.97	2388.06	TFCGTPEYLAPEVLEDNDYGR
278−298	2460.02	2459.01	2459.26	LENLMLDKDGHIKITDFGLC(Carb)K
291−298	953.45	952.44	952.47	ITDFGLC(Carb)K
291−308	1885.79	1884.78	1884.90	ITDFGLCKEGISDGATMK
309−329	2388.97	2387.96	2388.06	TFCGTPEYLAPEVLEDNDYGR
309−329	2446.01	2445.00	2445.08	TFC(Carb)GTPEYLAPEVLEDNDYGR
309−329	2547.11	2546.06	2546.19	TFC(**HNE**)GTPEYLAPEVLEDNDYGR
330−347	2159.88	2158.87	2158.95	AVDWWGLGVVMYEMMC(Carb)GR
330−347	2175.90	2174.90	2174.94	AVDWWGLGVVMYEMM(Ox)C(Carb)GR
330−347	2191.86	2190.86	2190.94	AVDWWGLGVVMYEM(Ox)M(Ox)C(Carb)GR
330−347	2207.87	2206.86	2206.93	AVDWWGLGVVM(Ox)YEM(Ox)M(Ox)C(Carb)GR
348−357	1318.58	1317.57	1317.61	LPFYNQDHER
358−368	1405.73	1404.72	1404.77	LFELILMEEIR
379−386	814.51	813.50	813.53	SLLAGLLK
391−407	1882.89	1881.88	1881.91	QRLGGGPSDAKEVM(Ox)EHR
393−401	801.40	800.39	800.4	LGGGPSDAK
408−420	1623.80	1622.79	1622.85	FFLSINWQDVVQK
421−437	1955.06	1954.05	1954.09	KLLPPFKPQVTSEVDTR
422−437	1826.94	1825.93	1825.99	LLPPFKPQVTSEVDTR

Table 1. Continued

start−end	observed[b]	M_r(expt)[c]	M_r(calc)[d]	sequence[e]
438−455	2115.92	2114.91	2114.98	YFDDEFTAQSITITPPDR
456−467	1421.72	1420.71	1420.72	YDSLGLLELDQR

[a] Twenty micrograms of rAkt2 was treated with 4-HNE (molar ratio of 1:1), digested with trypsin, and analyzed using MALDI-TOF/TOF as described in Experimental Procedures. Peptides containing a 4-HNE adduct at amino acids His196, His267, and Cys311 are denoted in bold. [b] Observed is the experimental m/z value. [c] M_r(expt) is the experimental m/z value transformed to a relative molecular mass. [d] M_r(calc) is the relative molecular mass calculated from the matched peptide sequence. [e] Carb, cysteine carbamidomethyl; Ox, methionine oxidation.

indicates an increase in the total levels of Akt, Akt2, and GSK3β carbonylation following cellular treatment with 4-HNE. Subsequent quantification of the Western blots demonstrates a 40-fold increase in carbonylated total Akt and Akt2 and a 3-fold increase in aldehyde-modified GSK3β in 4-HNE-treated cells as compared to controls (Figure 6B−D). As a control, the ability of 4-HNE to lead to an increased level of carbonylation of acetyl-CoA carboxylase (ACC) in HepG2 cells was also examined. 4-HNE treatment of HepG2 cells did not lead to an increase in the level of carbonylation of ACC (data not shown). These data clearly indicate that intracellular carbonylation of Akt, Akt2, and GSK3β readily occurs as a consequence of 4-HNE exposure.[8]

GSK3β Activity Is Not Inhibited by 4-HNE in HepG2 Cells. In normal cells, Akt phosphorylation of GSK3β inhibits GSK3β-dependent phosphorylation of glycogen synthase, enhancing glycogen synthesis.[16] Previous studies in other cell types have also indicated 4-HNE mediated inhibition of GSK3β activity.[31] To ascertain the effects of 4-HNE on GSK3β downstream signaling, we assessed a time course using cells treated with 100 μM 4-HNE, after which GSK3β-dependent phosphorylation of Ser641 on glycogen synthase was examined. From Figure 6E, treatment with 4-HNE leads to an increase in the level of glycogen synthase phosphorylation compared to controls. These data suggest that although GSK3β is carbonylated following 4-HNE treatment, GSK3β activity is not inhibited.

4-HNE Modifies and Inhibits Akt2 Activity in Vitro. To determine the direct effects of 4-HNE on Akt2, recombinant constitutively active myristoylated Akt2 (rAkt2) was expressed, purified, and incubated with increasing molar ratios of 4-HNE.[32] The 4-HNE modification quantified by Western blotting is presented in Figure 7A in conjunction with the effects of 4-HNE on rAkt2 activity (Figure 7B), which were examined using a GST-GSK3β fusion peptide as previously described in Experimental Procedures. From the Western blot, increasing 4-HNE:rAkt2 molar ratios or molar concentrations of 4-HNE lead to increased levels of modification of rAkt2. Quantification of the Western blots indicates a linear response in antibody reactivity correlating to an increased level of protein modification (Figure 7A). When activity assays were performed, Akt activity was significantly decreased at molar ratios of 5:1 (30%) and 10:1 (85%) (Figure 7B). Combined, these data indicate modification of rAkt2 and inhibition of rAkt2 activity by 4-HNE.

Identification of 4-HNE-Modified His196, His267, and Cys311 in Recombinant Akt2 as Targets of 4-HNE Modification. Concentrations of Akt2 within the cell are not sufficient to definitively identify the sites of 4-HNE modification. Therefore, to identify specific residues in Akt2 modified by 4-HNE, rAkt2 was treated with increasing molar ratios of 4-HNE followed by SDS−PAGE, band excision, tryptic digestion, and MALDI-TOF/TOF analysis. From the trypsin digest, an average of 88% coverage was obtained (Figure 1 of the Supporting Information). The resulting peptides obtained and their respective m/z ratios (mass-to-charge ratio) are listed in Table 1. From Table 1, Cys311 at m/z 2547.11, His196 at m/z 1401.66, and His267 at m/z 2013.003 were identified as targets for 4-HNE modification. The MS spectra in Figure 8B show the resulting parent MS envelope at m/z 2547.11 corresponding to a 4-HNE-modified tryptic peptide containing Cys311 of rAkt2. Additionally, the characteristic MS/MS b/y ion fragmentation for that specific peptide confirms that Cys311 is the target residue of 4-HNE adduction. Alkylation of His196, His267, and Cys311 was subsequently confirmed using LC−MS (data not shown). These results identify His196, His267, and Cys311 as sites of 4-HNE modification on Akt2 at a molar ratio of 1:1.

Effects of 4-HNE Modification on Akt2 Structure and Peptide Binding. Computation-based minimization simulations were performed using the crystal structure of Akt2 bound to a synthetic GSK3β peptide and the ATP analogue AMP-PNP (Figure 9A,B).[26] The synthetic GSK3β peptide and the ATP analogue AMP-PNP were removed from the complex, and 4-HNE was adducted to Cys311 of Akt2. The adducted protein was subsequently subjected to minimization. In Figure 9A, the addition of 4-HNE on Cys311 via a Michael addition leads to a stable 4-HNE adduct that extends into the peptide binding cleft of Akt2. From Figure 9B, 4-HNE modification of Cys311 does not prevent access of PDK1 and mTORC2 to Thr309 or Ser474, thus allowing for phosphorylation. The synthetic GSK3β peptide and the ATP analogue AMP-PNP were reintroduced into the minimized 4-HNE-adducted Akt2 protein structure to examine the accessibility of the respective binding sites. In Figure 9C, modeling the effects of alkylation of Cys311 by 4-HNE with respect to the ATP analogue (AMP-PNP) and the GSK3α/β peptide demonstrates the inability of the peptide substrate to interact with the substrate binding cleft. From the top view, 4-HNE prevents the interaction of Phe10 and Ala11 in the GSK3$\alpha\beta$ peptide with the substrate binding pocket of Akt2 (Figure 2 of the Supporting Information).

On the basis of the structural information obtained from the modeling simulation, His267 is located in the periphery of Akt2 17.9 Å from the active site and the face of Akt2 that interacts with the PH domain (Figure 3A of the Supporting Information). His196 is located adjacent to Cys311 along the rim of the active site cleft of Akt2. Because of the orientation of His196, there are two possible mechanisms of 4-HNE modification. In Figure 4A of the Supporting Information, 4-HNE modification of His196 occurs with the alkyl tail of 4-HNE extending along the active site cleft with the aldehyde group extending toward Thr309. In Figure 4B of the Supporting Information, His196-bound 4-HNE is oriented with the alkyl tail of 4-HNE extending out of the active site cleft and the aldehyde moiety

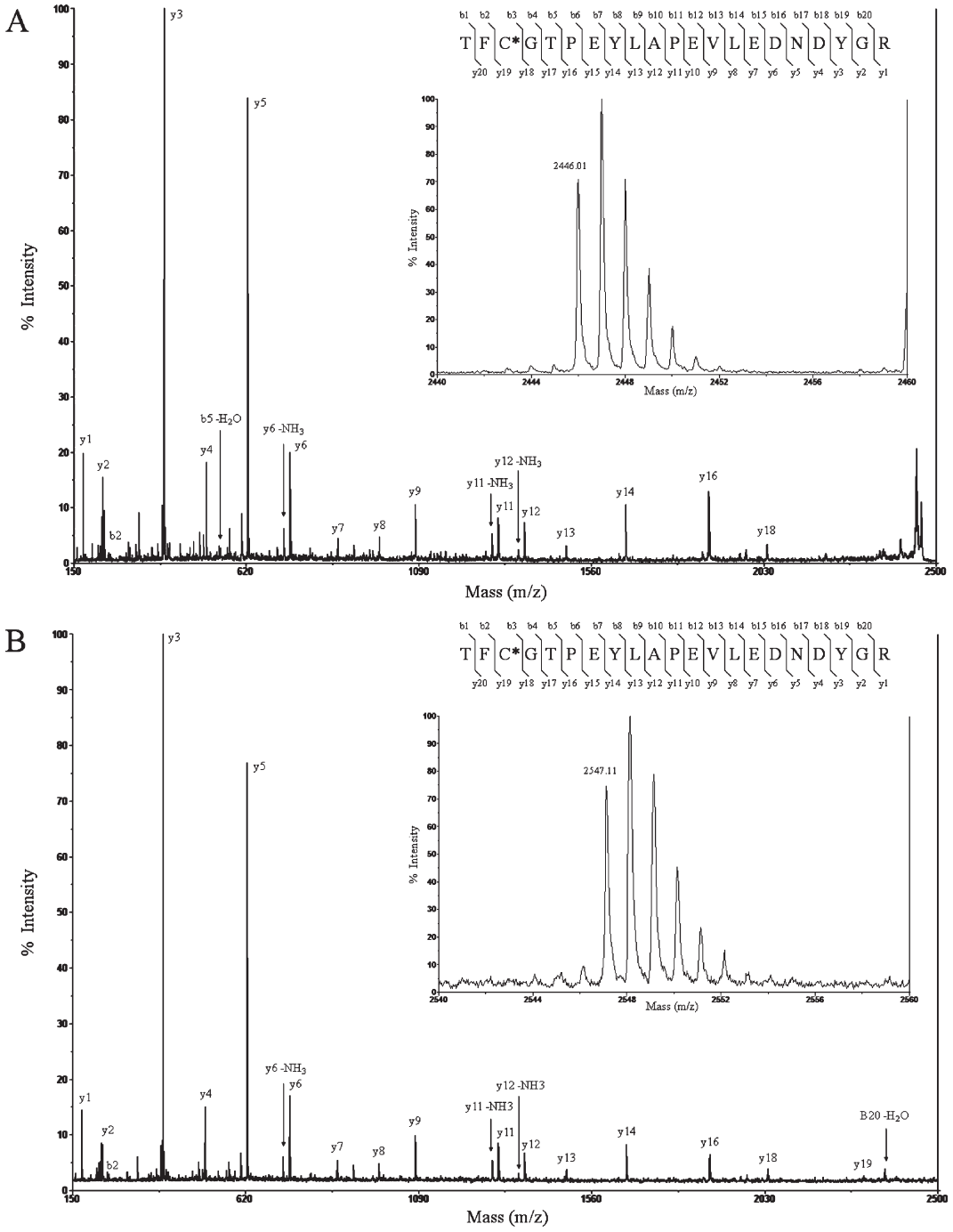

Figure 8. Identification of 4-HNE-modified rAkt2 at residue Cys311. Twenty micrograms of rAkt was treated with 4-HNE at a molar ratio of 1:1 (3.9 μM) and processed as previously described. (A) MS analysis of control rAkt2 revealed a peak envelope with a molecular mass (m/z) of 2446.01 (inset), corresponding to the Cys311 containing tryptic peptide with a carbamidomethyl-Cys addition. MS/MS was performed, and the resulting b/y ion fragmentation confirmed the peptide identity. (B) MS analysis of 4-HNE-modified rAkt2 revealed a peak envelope with a molecular mass (m/z) of 2547.11 (inset), corresponding to the Cys311-containing tryptic peptide with a reduced 4-HNE-Cys modification. MS/MS was performed, and the resulting b/y ion fragmentation confirmed the peptide identity.

extending into the cleft. Although it is impossible to determine which of these possible conformations actually occur, both of these conformations will block access of the substrate to the active site cleft. Combined, these data demonstrate a mechanism of 4-HNE-mediated inhibition of Akt2 whereby the binding of the peptide substrate to Akt2 is sterically restricted by 4-HNE.

DISCUSSION

Under conditions of sustained oxidative stress and inflammation, 4-HNE is proposed to initiate cellular damage and to promote cellular survival.[33] These processes have been demonstrated to occur simultaneously. Treatment of HepG2 cells with micromolar concentrations of 4-HNE has been demonstrated to

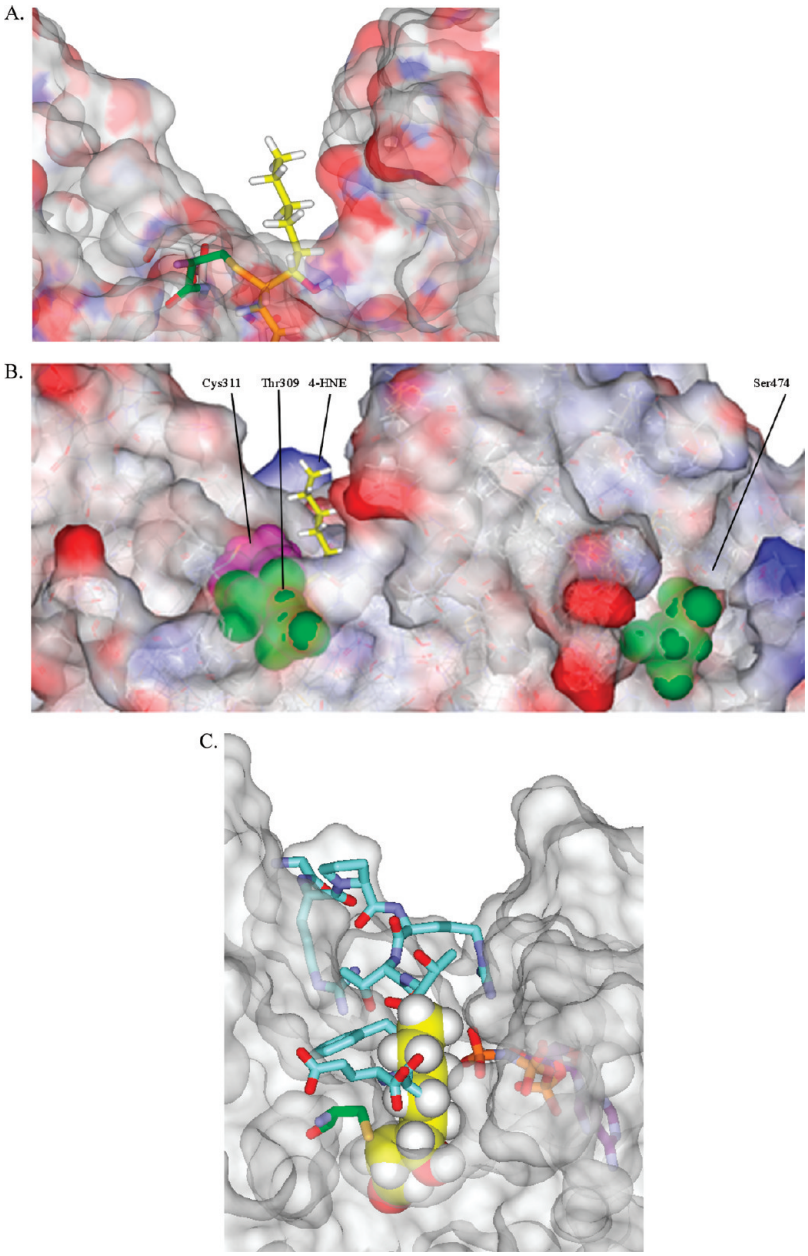

Figure 9. Molecular modeling of 4-HNE-modified Cys311 on Akt2. (A) Electron density map of the Akt2 protein surface with 4-HNE-modified Cys311 (4-HNE colored yellow). (B) Relationship of 4-HNE-modified Cys311, Thr309, and Asp474 (4-HNE colored yellow, Cys311 colored magenta, and Thr309 and Asp474 colored green). (C) Overlay of the AMP-PNP ATP analogue and GSK3β peptide into the active site of 4-HNE-adducted Akt2 [carbon atoms of 4-HNE colored yellow, Cys311 colored green, AMP-PNP ATP colored purple (nucleotide) or orange (phosphate), and GSK3β peptide colored cyan].

promote cell survival by cytosolic translocation of Daxx and the upregulation of protective factors such as GSTA4-4 and Hsp70.[34] In the same cells, 4-HNE promoted apoptosis via a Fas-mediated extrinsic pathway.[33] In other studies, 4-HNE downregulated Akt by promoting dephosphorylation by PP2A enhancing apoptosis.[25] Thus, the downstream effects of 4-HNE are multifactorial and cell type specific.

Insulin signaling in the liver is essential for the maintenance of glucose homeostasis. The inability of the hepatocytes to respond to insulin is a well-documented phenotype in many chronic hepatic diseases, including ALD, NASH, and hepatitis C.[35−37] Likewise, in models of chronic exposure, increased oxidative stress correlates with insulin resistance.[38] Although the exact mechanisms are not completely known, inhibition of insulin-dependent Akt signaling is a contributing factor. Mutations of Akt2 in humans manifest as severe insulin resistance and diabetes.[39] Therefore, understanding the interaction of 4-HNE with insulin-dependent cellular pathways is essential to understanding the pathogenesis of chronic diseases associated with oxidative stress. In this report, we characterize the effects of 4-HNE on insulin-mediated Akt activation and downstream signaling in HepG2 cells.

Both Akt1 and Akt2 are implicated in cell growth and in the regulation of the cell cycle.[40] In adipocytes, insulin stimulation

promotes plasma membrane association of Akt2 but not Akt1, yet both have roles in GSK3β regulation.[41] Very little is known concerning Akt isoform responses due to oxidative stress. Akt2 has been shown to be activated following micromolar level exposure to hydrogen peroxide.[20] In hepatocytes, exposure to 4-HNE does not lead to the production of reactive oxidative species (ROS).[12] The effects of 4-HNE on Akt isoforms was not investigated in those studies. Therefore, these studies were performed to improve our understanding of the specific Akt isoform phosphorylated following 4-HNE exposure. In Figure 2, insulin led to phosphorylation of both Akt1 and Akt2 whereas 4-HNE treatment increased the level of phosphorylation of only Akt2 (not Akt1). This suggests that only Akt2 is phosphorylated following 4-HNE stimulation. Combined, these data indicate that ROS are not involved in Akt2 activation by 4-HNE.

Phosphorylation of Akt inactivates GSK3β downstream signaling, resulting in an increased level of glycogen synthesis via glycogen synthase. In the dephosphorylated state, GSK3β is active and will phosphorylate GS, leading to inhibition of glycogen synthesis. Studies have previously demonstrated increased levels of 4-HNE-dependent Akt phosphorylation of GSK3β and activation of β-catenin in both neuroblastoma and MCF-7 cells.[31,42] Surprisingly, in Figures 3 and 4, 4-HNE treatment significantly decreased the level of Akt-dependent GSK3β (Ser9) phosphorylation compared to that of untreated cells and prevented the ability of insulin to stimulate GSK3β phosphorylation as well. GSK3β activity was not affected as determined by the increased level of phosphorylation of GS (Figure 6).

Insulin also promotes enhanced cell survival by phosphorylation of the ubiquitin ligase protein Mdm2 by Akt2. This in turn leads to an increased level of degradation of p53 because of its ubiquitination. In prostate epithelial cells, depletion of mitochondrial DNA led to Akt2 activation, MDM2 phosphorylation, and glucose uptake.[20] In HepG2 cells, insulin stimulation led to an increased level of MDM2 phosphorylation.[43] In Figure 4, treatment with insulin led to a 2-fold increase in the level of phosphorylation on p-MDM2 (Ser166). Following 4-HNE pretreatment, the level of MDM2 phosphorylation is significantly decreased below levels of untreated cells. Using in vitro Akt kinase activity assays, the data in Figure 5 clearly demonstrate a significant decrease in Akt activity below that of unstimulated cells. Combined with the decrease in the level of GSK3β phosphorylation, these data clearly indicate inhibition of Akt-dependent downstream activity by 4-HNE.

It should be noted that we have been unable to detect apoptosis following 4-HNE treatment,[44] suggesting that other pro-survival pathways in addition to the Akt pathway are activated by 4-HNE. The protein kinases Erk1/2 are known regulators of cell proliferation. Stimulation of HepG2 cells with IGF1 increased the level of Erk1/2 phosphorylation and proliferation in an insulin receptor substrate 4-dependent mechanism.[45] The data in Figure 3 demonstrate 4-HNE stimulation of Erk1/2 phosphorylation in HepG2 cells. This provides an alternative mechanism for increased cell survival following 4-HNE treatment.

Recent proteomic studies have identified numerous protein targets of 4-HNE in cells. Using 4-HNE concentrations of 50 and 100 μM in RKO cells, more than 1500 different proteins were identified using streptavidin capture of biotinamidohexanoic acid hydrazide-treated lysates followed by liquid chromatography and tandem mass spectrometry.[30] In MCF-7 cells, another member of the AGC kinase family (LKB1) was identified as a direct target of 4-HNE.[46] Mutational studies identified a critical cysteine residue (Cys210) within the activation loop of LKB1 that is alkylated by 4-HNE. Data presented in this study clearly indicate that Akt2 is also a target of 4-HNE. The data in Figure 6 indicate that using biotin hydrazide capture, the levels of alkylation and carbonylation of Akt2 are significantly increased following 4-HNE treatment in HepG2 cells. In addition, these experiments using recombinant Akt2 and LC−MS identify His196 (located along the active site cleft), His267 (located on the periphery of Akt2), and Cys311 within the activation loop as selective targets of alkylation of Akt2 by 4-HNE at molar ratios of 1:1 (Figure 8 and Table 1 and Figures 2−4 of the Supporting Information). Further, in Figure 7, increasing molar ratios and concentrations of 4-HNE also lead to inhibition of rAkt2 activity.

In this study, identification of the Akt2 His196, His267, and Cys311 residues modified by Michael addition of 4-HNE suggests some intriguing possibilities concerning the mechanism of 4-HNE-mediated Akt2 inhibition. Both His196 and His267 have not previously been studied in detail. His267 is not located in the active site. Examining the distance between the α-carbon of His196 and the α-carbon of His267 indicates a distance of 17.9 Å (Figure 3A of the Supporting Information). Therefore, modification of His267 should not affect activity. Both His196 and Cys311 are located on or near the lip of the active site cleft and on the C-terminal side of the activation loop of Akt2, respectively. Under oxidizing conditions, Cys311 is covalently linked to Cys297 via a disulfide linkage.[47] Once active, this linkage cannot exist, as the activation loop is shifted. Studies suggest that Cys311 governs enzyme−substrate interaction by coordinating residue P + 1 of the substrate.[47] Akt2 modeling studies depicted in Figure 9 and Figures 2 and 4 of the Supporting Information suggest modification of Cys311 or His196 with 4-HNE sterically blocks access of the peptide substrate, but it does not prevent phosphorylation at Thr309 or Ser474. Both Thr309 and Ser474 are still exposed to the solvent and could be phosphorylated by PDK1 and mTORC2.[16] When Akt2 is not bound to the membrane, the PH-in conformation allosterically prevents phosphorylation and also would prevent 4-HNE interaction. In Figure 3B of the Supporting Information, the interaction of Trp80 in the PH domain and Lys298, Glu299, and Glu315 of the catalytic domain blocks the access of 4-HNE to His196 and Cys311. The molecular interaction of the PH domain of Akt2 with the membrane creates a PH-out conformation that would subsequently allow access to His196 or Cys311 by 4-HNE, regardless of phosphorylation status. It should also be noted because of its lipophilic nature, concentrations of 4-HNE are highest within membranes. In vivo localized membrane concentrations of reactive aldehydes from livers isolated from CCl_4- and $BrCCl_3$-treated rats were 3.8 and 11.3 mM, respectively.[8,48,49] These pathophysiological concentrations are significantly higher than concentrations used in this study and indicate the in vivo relevance of these experimental results. Thus, although Akt2 is phosphorylated following 4-HNE treatment in cells, its activity is subsequently inhibited by direct 4-HNE modification at the membrane. This provides a mechanism of Akt2 phosphorylation on Thr309 and Ser474 and concurrent inhibition by 4-HNE.

Chronic inflammation, and the associated oxidative stress leading to production of reactive oxidative species such as 4-HNE, are important components of many hepatic diseases, including NASH and ALD. In addition to steatosis, one of the clinical manifestations

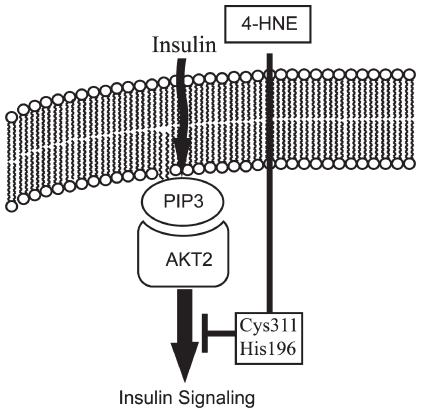

Figure 10. Model of the effects of 4-HNE on insulin signaling in HepG2 cells. Under normal conditions, insulin stimulates Akt2 phosphorylation at Thr309 and Ser474. This leads to an increased level of glycogen synthesis and an increased level of cell survival. Under conditions of chronic inflammation, Akt2 is carbonylated by 4-HNE inhibiting activity. This prevents insulin-stimulated glycogen synthesis enhancing insulin resistance and leads to a possibly decreased level of cell survival.

of these diseases is an insulin resistant state. On the basis of the results presented in this study using HepG2 cells as a model, we propose that 4-HNE inhibits insulin-dependent signaling downstream of Akt2 (Figure 10). Under normal conditions, Akt2 phosphorylates both GSK3β and MDM2, leading to an increase in the levels of glycogen synthesis and cell survival. However, during chronic inflammation and oxidative stress, Akt2 is recruited to the membrane and activated by phosphorylation of Thr309 and Ser474. Concurrently, the production of 4-HNE within the lipid bilayer leads to direct modification of Akt2 on Cys311 by 4-HNE, preventing substrate binding and inhibiting activity. Thus, the inhibition of Akt2 due to 4-HNE modification could contribute to insulin resistance in inflammatory liver disease. It should be stressed that in our model, Akt2 is modified by 4-HNE regardless of Akt2 phosphorylation. Therefore, these data also suggest a need for caution when interpreting Akt activation during conditions of increased oxidative stress.

■ ASSOCIATED CONTENT

Supporting Information. Additional materials and data. This material is available free of charge via the Internet at http://pubs.acs.org.

■ AUTHOR INFORMATION

Corresponding Author

*Department of Pharmaceutical Sciences, School of Pharmacy, University of Colorado—Denver, 12700 E. 19th Ave., Box C238, Building P15, Room 3113, Aurora, CO 80045. Phone: (303) 724-3397. Fax: (303) 724-7266. E-mail: dennis.petersen@ucdenver.edu.

Funding Sources

Supported by National Institutes of Health Grants F32 AA018613-01A1 (C.T.S.) and R37AA009300-14 (D.R.P.).

■ ACKNOWLEDGMENT

We thank Dr. Rajesh Agarwal (University of Colorado—Denver) for his assistance in review of the manuscript.

■ ABBREVIATIONS

ALD, alcoholic liver disease; Glut4, glucose transporter type 4; GSK3β, glycogen synthase kinase 3β; 4-HNE, 4-hydroxy-2-nonenal; IRS-1 and IRS-2, insulin receptor substrates 1 and 2, respectively; MALDI-TOF/TOF, matrix-assisted laser desorption ionization time-of-flight tandem mass spectrometry; NASH, non-alcoholic steatohepatitis; PDK-1, phosphoinositide-dependent kinase 1; PI3K, phosphatidylinositol 3-kinase; PtdIns(3,4,5)P_3, phosphatidylinositol 3,4,5-trisphosphate; PH, pleckstrin homology; PP2A, protein phosphatase 2A; PTEN, phosphatase and tensin homologue from which chromosome 10 has been deleted; MDM2, ubiquitin ligase murine double minute oncogene 2; SDS−PAGE, sodium dodecyl sulfate−polyacrylamide gel electrophoresis.

■ REFERENCES

(1) Paradis, V., Kollinger, M., Fabre, M., Holstege, A., Poynard, T., and Bedossa, P. (1997) In situ detection of lipid peroxidation by-products in chronic liver diseases. *Hepatology 26*, 135–142.

(2) Paradis, V., Mathurin, P., Kollinger, M., Imbert-Bismut, F., Charlotte, F., Piton, A., Opolon, P., Holstege, A., Poynard, T., and Bedossa, P. (1997) In situ detection of lipid peroxidation in chronic hepatitis C: Correlation with pathological features. *J. Clin. Pathol. 50*, 401–406.

(3) Roede, J. R., Orlicky, D. J., Fisher, A. B., and Petersen, D. R. (2009) Overexpression of peroxiredoxin 6 does not prevent ethanol-mediated oxidative stress and may play a role in hepatic lipid accumulation. *J. Pharmacol. Exp. Ther. 330*, 79–88.

(4) Roede, J. R., Stewart, B. J., and Petersen, D. R. (2008) Decreased expression of peroxiredoxin 6 in a mouse model of ethanol consumption. *Free Radical Biol. Med. 45*, 1551–1558.

(5) Sampey, B. P., Korourian, S., Ronis, M. J., Badger, T. M., and Petersen, D. R. (2003) Immunohistochemical characterization of hepatic malondialdehyde and 4-hydroxynonenal modified proteins during early stages of ethanol-induced liver injury. *Alcohol.: Clin. Exp. Res. 27*, 1015–1022.

(6) Kohli, R., Kirby, M., Xanthakos, S. A., Softic, S., Feldstein, A. E., Saxena, V., Tang, P. H., Miles, L., Miles, M. V., Balistreri, W. F., Woods, S. C., and Seeley, R. J. (2010) High-fructose, medium chain trans fat diet induces liver fibrosis and elevates plasma coenzyme Q9 in a novel murine model of obesity and nonalcoholic steatohepatitis. *Hepatology 52*, 934–944.

(7) Schaur, R. J. (2003) Basic aspects of the biochemical reactivity of 4-hydroxynonenal. *Mol. Aspects Med. 24*, 149–159.

(8) Benedetti, A., Comporti, M., Fulceri, R., and Esterbauer, H. (1984) Cytotoxic aldehydes originating from the peroxidation of liver microsomal lipids. Identification of 4,5-dihydroxydecenal. *Biochim. Biophys. Acta 792*, 172–181.

(9) Esterbauer, H., Schaur, R. J., and Zollner, H. (1991) Chemistry and biochemistry of 4-hydroxynonenal, malonaldehyde and related aldehydes. *Free Radical Biol. Med. 11*, 81–128.

(10) Roede, J. R., Carbone, D. L., Doorn, J. A., Kirichenko, O. V., Reigan, P., and Petersen, D. R. (2008) In Vitro and in Silico Characterization of Peroxiredoxin 6 Modified by 4-Hydroxynonenal and 4-Oxononenal. *Chem. Res. Toxicol. 21*, 2289–2299.

(11) Stewart, B. J., Doorn, J. A., and Petersen, D. R. (2007) Residue-specific adduction of tubulin by 4-hydroxynonenal and 4-oxononenal causes cross-linking and inhibits polymerization. *Chem. Res. Toxicol. 20*, 1111–1119.

(12) Shearn, C. T., Smathers, R. L., Stewart, B. J., Fritz, K. S., Galligan, J. J., Hail, N., and Petersen, D. R. (2011) PTEN Inhibition by 4-Hydroxynonenal Leads to Increased Akt Activation in Hepatocytes. *Mol. Pharmacol.*, in press.

(13) Calleja, V., Alcor, D., Laguerre, M., Park, J., Vojnovic, B., Hemmings, B. A., Downward, J., Parker, P. J., and Larijani, B. (2007) Intramolecular and intermolecular interactions of protein kinase B define its activation in vivo. *PLoS Biol. 5*, e95.

(14) Wu, W. I., Voegtli, W. C., Sturgis, H. L., Dizon, F. P., Vigers, G. P., and Brandhuber, B. J. (2010) Crystal structure of human AKT1

with an allosteric inhibitor reveals a new mode of kinase inhibition. *PLoS One 5*, e12913.

(15) Calleja, V., Laguerre, M., and Larijani, B. (2009) 3-D structure and dynamics of protein kinase B: New mechanism for the allosteric regulation of an AGC kinase. *J. Chem. Biol. 2*, 11–25.

(16) Liao, Y., and Hung, M. C. (2010) Physiological regulation of Akt activity and stability. *Am. J. Transl. Res. 2*, 19–42.

(17) Leavens, K. F., Easton, R. M., Shulman, G. I., Previs, S. F., and Birnbaum, M. J. (2009) Akt2 is required for hepatic lipid accumulation in models of insulin resistance. *Cell Metab. 10*, 405–418.

(18) Samuel, V. T., Petersen, K. F., and Shulman, G. I. (2010) Lipid-induced insulin resistance: Unravelling the mechanism. *Lancet 375*, 2267–2277.

(19) Katome, T., Obata, T., Matsushima, R., Masuyama, N., Cantley, L. C., Gotoh, Y., Kishi, K., Shiota, H., and Ebina, Y. (2003) Use of RNA interference-mediated gene silencing and adenoviral overexpression to elucidate the roles of AKT/protein kinase B isoforms in insulin actions. *J. Biol. Chem. 278*, 28312–28323.

(20) Moro, L., Arbini, A. A., Yao, J. L., di Sant'Agnese, P. A., Marra, E., and Greco, M. (2009) Mitochondrial DNA depletion in prostate epithelial cells promotes anoikis resistance and invasion through activation of PI3K/Akt2. *Cell Death Differ. 16*, 571–583.

(21) Cho, H., Mu, J., Kim, J. K., Thorvaldsen, J. L., Chu, Q., Crenshaw, E. B., III, Kaestner, K. H., Bartolomei, M. S., Shulman, G. I., and Birnbaum, M. J. (2001) Insulin resistance and a diabetes mellitus-like syndrome in mice lacking the protein kinase Akt2 (PKB β). *Science 292*, 1728–1731.

(22) Stiles, B., Wang, Y., Stahl, A., Bassilian, S., Lee, W. P., Kim, Y. J., Sherwin, R., Devaskar, S., Lesche, R., Magnuson, M. A., and Wu, H. (2004) Liver-specific deletion of negative regulator Pten results in fatty liver and insulin hypersensitivity [corrected]. *Proc. Natl. Acad. Sci. U.S.A. 101*, 2082–2087.

(23) He, L., Hou, X., Kanel, G., Zeng, N., Galicia, V., Wang, Y., Yang, J., Wu, H., Birnbaum, M. J., and Stiles, B. L. (2010) The critical role of AKT2 in hepatic steatosis induced by PTEN loss. *Am. J. Pathol. 176*, 2302–2308.

(24) He, J., de la Monte, S., and Wands, J. R. (2007) Acute ethanol exposure inhibits insulin signaling in the liver. *Hepatology 46*, 1791–1800.

(25) Liu, W., Akhand, A. A., Takeda, K., Kawamoto, Y., Itoigawa, M., Kato, M., Suzuki, H., Ishikawa, N., and Nakashima, I. (2003) Protein phosphatase 2A-linked and -unlinked caspase-dependent pathways for downregulation of Akt kinase triggered by 4-hydroxynonenal. *Cell Death Differ. 10*, 772–781.

(26) Yang, J., Cron, P., Good, V. M., Thompson, V., Hemmings, B. A., and Barford, D. (2002) Crystal structure of an activated Akt/protein kinase B ternary complex with GSK3-peptide and AMP-PNP. *Nat. Struct. Biol. 9*, 940–944.

(27) Brooks, B. R., III, Brooks, C. L., Mackerell, A. D., Jr., Nilsson, L., Petrella, R. J., Roux, B., Won, Y., Archontis, G., Bartels, C., Boresch, S., Caflisch, A., Caves, L., Cui, Q., Dinner, A. R., Feig, M., Fischer, S., Gao, J., Hodoscek, M., Im, W., Kuczera, K., Lazaridis, T., Ma, J., Ovchinnikov, V., Paci, E., Pastor, R. W., Post, C. B., Pu, J. Z., Schaefer, M., Tidor, B., Venable, R. M., Woodcock, H. L., Wu, X., Yang, W., York, D. M., and Karplus, M. (2009) CHARMM: The biomolecular simulation program. *J. Comput. Chem. 30*, 1545–1614.

(28) Onufriev, A., Case, D. A., and Bashford, D. (2002) Effective Born radii in the generalized Born approximation: The importance of being perfect. *J. Comput. Chem. 23*, 1297–1304.

(29) Ramos, J. W. (2008) The regulation of extracellular signal-regulated kinase (ERK) in mammalian cells. *Int. J. Biochem. Cell Biol. 40*, 2707–2719.

(30) Codreanu, S. G., Zhang, B., Sobecki, S. M., Billheimer, D. D., and Liebler, D. C. (2009) Global analysis of protein damage by the lipid electrophile 4-hydroxy-2-nonenal. *Mol. Cell. Proteomics 8*, 670–680.

(31) Dozza, B., Smith, M. A., Perry, G., Tabaton, M., and Strocchi, P. (2004) Regulation of glycogen synthase kinase-3β by products of lipid peroxidation in human neuroblastoma cells. *J. Neurochem. 89*, 1224–1232.

(32) Gao, X., Yo, P., and Harris, T. K. (2005) Improved yields for baculovirus-mediated expression of human His_6-PDK1 and His_6-PKBβ/Akt2 and characterization of phospho-specific isoforms for design of inhibitors that stabilize inactive conformations. *Protein Expression Purif. 43*, 44–56.

(33) Chaudhary, P., Sharma, R., Sharma, A., Vatsyayan, R., Yadav, S., Singhal, S. S., Rauniyar, N., Prokai, L., Awasthi, S., and Awasthi, Y. C. (2010) Mechanisms of 4-hydroxy-2-nonenal induced pro- and anti-apoptotic signaling. *Biochemistry 49*, 6263–6275.

(34) Sharma, R., Sharma, A., Dwivedi, S., Zimniak, P., Awasthi, S., and Awasthi, Y. C. (2008) 4-Hydroxynonenal self-limits fas-mediated DISC-independent apoptosis by promoting export of Daxx from the nucleus to the cytosol and its binding to Fas. *Biochemistry 47*, 143–156.

(35) Kawaguchi, T., and Sata, M. (2010) Importance of hepatitis C virus-associated insulin resistance: Therapeutic strategies for insulin sensitization. *World J. Gastroenterol. 16*, 1943–1952.

(36) Lockman, K. A., and Nyirenda, M. J. (2010) Interrelationships between hepatic fat and insulin resistance in non-alcoholic fatty liver disease. *Curr. Diabetes Rev. 6*, 341–347.

(37) de la Monte, S. M., Yeon, J. E., Tong, M., Longato, L., Chaudhry, R., Pang, M. Y., Duan, K., and Wands, J. R. (2008) Insulin resistance in experimental alcohol-induced liver disease. *J. Gastroenterol. Hepatol. 23*, e477–e486.

(38) Derdak, Z., Lang, C. H., Villegas, K. A., Tong, M., Mark, N. M., de la Monte, S. M., and Wands, J. R. (2010) Activation of p53 enhances apoptosis and insulin resistance in a rat model of alcoholic liver disease. *J. Hepatol. 54*, 164–172.

(39) George, S., Rochford, J. J., Wolfrum, C., Gray, S. L., Schinner, S., Wilson, J. C., Soos, M. A., Murgatroyd, P. R., Williams, R. M., Acerini, C. L., Dunger, D. B., Barford, D., Umpleby, A. M., Wareham, N. J., Davies, H. A., Schafer, A. J., Stoffel, M., O'Rahilly, S., and Barroso, I. (2004) A family with severe insulin resistance and diabetes due to a mutation in AKT2. *Science 304*, 1325–1328.

(40) Yun, S. J., Tucker, D. F., Kim, E. K., Kim, M. S., Do, K. H., Ha, J. M., Lee, S. Y., Yun, J., Kim, C. D., Birnbaum, M. J., and Bae, S. S. (2009) Differential regulation of Akt/protein kinase B isoforms during cell cycle progression. *FEBS Lett. 583*, 685–690.

(41) Gonzalez, E., and McGraw, T. E. (2009) Insulin-modulated Akt subcellular localization determines Akt isoform-specific signaling. *Proc. Natl. Acad. Sci. U.S.A. 106*, 7004–7009.

(42) Covey, T. M., Edes, K., and Fitzpatrick, F. A. (2007) Akt activation by arachidonic acid metabolism occurs via oxidation and inactivation of PTEN tumor suppressor. *Oncogene 26*, 5784–5792.

(43) Paajarvi, G., Roudier, E., Crisby, M., Hogberg, J., and Stenius, U. (2005) HMG-CoA reductase inhibitors, statins, induce phosphorylation of Mdm2 and attenuate the p53 response to DNA damage. *FASEB J. 19*, 476–478.

(44) Stewart, B. J., Roede, J. R., Doorn, J. A., and Petersen, D. R. (2009) Lipid aldehyde-mediated cross-linking of apolipoprotein B-100 inhibits secretion from HepG2 cells. *Biochim. Biophys. Acta 1791*, 772–780.

(45) Cuevas, E. P., Escribano, O., Chiloeches, A., Ramirez Rubio, S., Roman, I. D., Fernandez-Moreno, M. D., and Guijarro, L. G. (2007) Role of insulin receptor substrate-4 in IGF-I-stimulated HEPG2 proliferation. *J. Hepatol. 46*, 1089–1098.

(46) Wagner, T. M., Mullally, J. E., and Fitzpatrick, F. A. (2006) Reactive lipid species from cyclooxygenase-2 inactivate tumor suppressor LKB1/STK11: Cyclopentenone prostaglandins and 4-hydroxy-2-nonenal covalently modify and inhibit the AMP-kinase kinase that modulates cellular energy homeostasis and protein translation. *J. Biol. Chem. 281*, 2598–2604.

(47) Huang, X., Begley, M., Morgenstern, K. A., Gu, Y., Rose, P., Zhao, H., and Zhu, X. (2003) Crystal structure of an inactive Akt2 kinase domain. *Structure 11*, 21–30.

(48) Benedetti, A., Fulceri, R., Ferrali, M., Ciccoli, L., Esterbauer, H., and Comporti, M. (1982) Detection of carbonyl functions in phospholipids of liver microsomes in CCl_4- and $BrCCl_3$-poisoned rats. *Biochim. Biophys. Acta 712*, 628–638.

(49) Benedetti, A., Esterbauer, H., Ferrali, M., Fulceri, R., and Comporti, M. (1982) Evidence for aldehydes bound to liver microsomal protein following CCl_4 or $BrCCl_3$ poisoning. *Biochim. Biophys. Acta 711*, 345–356.